Biointerface Research in Applied Chemistry
Open-Access Journal (ISSN: 2069-5837)

Article
Volume 14, Issue 5, 2024, 104
https://doi.org/10.33263/BRIAC145.104

Impact of E71S Mutation on SHANK3 Conformational Dynamics at the SPN-ARR Interface

Hiba Khalil Almaadani [1], Venkata Satish Kumar Mattaparthi [1,*]

[1] Molecular Modeling and Simulation Laboratory, Department of Molecular Biology and Biotechnology, Tezpur University, Tezpur, Assam, 784028, India; hiba.madanli@gmail.com (H.K.M.); mvenkatasatishkumar@gmail.com, venkata@tezu.ernet.in (V.S.K.M.)
* Correspondence: mvenkatasatishkumar@gmail.com, venkata@tezu.ernet.in (V.S.K.M.);
Scopus Author ID:54962670000
Received: 5.03.2024; Accepted: 12.05.2024; Published: 21.07.2024

Abstract: Autism spectrum disorder (ASD) is a complicated neurological condition. The genetic factors implicated in ASD have included a variety of loci that converge on neurological pathways, mainly excitatory synapses. SHANK3, a crucial protein in post-synaptic neuron cells, has been linked to ASD through mutations in the N-terminal, substantially the SPN domain. Our study aims to evaluate the influence of the E71S mutation on SHANK3, assessing its dynamics, stability, flexibility, and compactness compared to the SHANK3 WT. We employed molecular dynamics simulations to investigate the structural dynamics of both SHANK3 WT and the E71S mutant. Simulation steps encompassed heating dynamics, density equilibration, and production, followed by trajectory analysis, including RMSD, RMSF, Rg, B-factor, hydrogen bond interactions, and changes in secondary structure. The simulations unveiled that the E71S mutation perturbs the stability and folding of SHANK3, leading to the disturbance of intramolecular contacts between the SPN and ARR domains, consequently influencing the binding with αCaMKII and α-Fodrin to its sites on the SHANK3. These findings highlight the possible role of an open-up mutation between SPN-ARR tandem on dendritic spine shape and plasticity of synaptic neurons in neurodevelopmental disorders.

Keywords: autism spectrum disorder; SHANK3 gene; E71S mutation; molecular dynamics simulation; αCaMKII; α-Fodrin.

1. Introduction

Autism spectrum disorder (ASD) is a condition of neurological development that emerges during the first years of early childhood and is characterized by an array of stereotyped activities, delays in communication, and social interaction disturbances [1]. The current worldwide incidence of ASD is estimated to be around 100 cases per 10,000 individuals [2]. A variety of genetic loci have been associated with the pathomechanisms of ASD. However, these loci ultimately lead to limited neural circuits that are involved in aberrant communication at excitatory synapses [3]. Consequently, one of the key pathways underpinning the development of ASD has been postulated to be the alteration of post-synaptic neural excitation [4]. SH3 and multiple ankyrin repeat domains 3 (SHANK3) constitute a key protein in post-synaptic density (PSD). SHANK3 was extensively investigated in nerve cells as a scaffolding protein [5]. Abnormal variations and dysregulation in SHANK3 have been linked to ASD [6-8]. SHANK3 encompasses five distinct domains. The Shank/ProSAP N-terminal (SPN) domain has a conformation similar to a ubiquitin-like (Ubl) domain, analogous to how Ras association

domains. Previous research findings have established that activated Ras and Rap proteins exhibit elevated affinity to the SPN domain [9]. Furthermore, the SPN region bonds in close intramolecular interactions with the Ankyrin Repeat Region (ARR) or Ank domain, restricting the accessibility of α-Fodrin and Sharpin as known interaction partners of the Ank repeat [10]. Besides, the SH3 domain allows for interactions with AMPAR through GRIP. AMPARs, operating as ion channels, enhance fast synaptic communication and impact cognitive processes, including learning and memory [11]. Moreover, within SHANK3, a proline-rich region is situated among the C-terminal SAM and PDZ domains [12]. Point mutations have been spotlighted as prominent loci in the N-terminus [13]. Two autism-related mutations, R12C and L68P, in the SPN region impair SHANK3's interaction with Rap1, leading to a blockage in integrin activation [14, 15]. Experimental findings indicate that the N52R mutation exposes the ARR region, facilitating subsequent binding to external GFP-SPN. The N52R mutation also modifies the ASD-like symptoms SHANK3 regulates in vivo by either impairing or enhancing SHANK3's functional role in actin binding [16]. A lack of αCaMKII ligating appears to be a more common consequence of SHANK3 point variants, and a recent study proposed that this could be caused by N52R disruption of the SPN−ARR interface. According to their hypothesis, SHANK3's negative regulatory actions on the αCaMKII signaling pathway, which is highly involved in synaptic plasticity, may have a physiological impact on this relationship [17]. This study aims to generate a point mutation at position 71 in the SPN region and explore the effects of SHANK3 point mutation E71S on synapse plasticity, function, and structure. Using molecular dynamics (MD) simulations, the complex relationship between genetic variations and the E71S mutant relative to SHANK3 wild type (WT) in the context of ASD pathogenesis was clarified. Based on protein equilibrium, flexibility, and compactness, the stability of the SHANK3 WT and the SHANK3 E71S mutant structures were evaluated. The consequences of the deleterious mutation on protein binding sites—that is, those affecting neuronal transmission and synaptic plasticity—were then assessed.

2. Materials and Methods

2.1. Construction of primary structures.

2.1.1. SHANK3 protein**.**

Molecular dynamics simulation was performed using the SH3 and multiple ankyrin repeat domains 3 structure, PDB ID 5G4X [15], obtained from the RCSB Protein Data Bank [18].

2.1.2. Constructing the E71S SHANK3 mutant**.**

The principal configuration of the E71S mutant was created by manipulating the three-dimensional configuration of the scaffold protein WT SHANK3 (PDB ID: 5G4X). The Rotamer tool of the CHIMERA program [19] was utilized to build E71S SHANK3, where Glutamic acid was substituted with Serine at nucleotide 71 in the SPN domain of SHANK3.

2.2. Setup for molecular dynamics simulations.

SHANK3 E71S mutant and SHANK3 WT systems were constructed for the MD simulation utilizing ff99SBildn as a force field parameter in the Leap module of the AMBER 14 software package [20]. A prominent TIP3P water model [21] was applied as a solvent to

explicitly stated SHANK3 WT and SHANK3 E71S mutant systems independently utilizing a buffer dimension of 10 Å in a periodic cubic box. The charge of the SHANK3 WT and the SHANK3 E71S mutant structures have been neutralized by the addition of an adequate number of counter ions and, afterward, undergoing a reduction of energy to eliminate the London dispersion force.

The molecular dynamics simulation adheres to a consistent method comprising heating dynamics followed by density, equilibrium, and production dynamics. Initial structures were energy-minimized for further Molecular Dynamics procedures. The gradual heating of structures from 0 to 300 K occurred under a steady volume (NVT) situation, followed by the density approach. Equilibration was accomplished under NPT conditions (300 K and 1 atm pressure) for one nanosecond. Visualization of temperature and pressure analysis were undertaken to ensure correct equilibration. Subsequently, a 200 ns MD production run for stabilized structures using the PME algorithm [22, 23] with a time phase of 2 fs. A threshold of 8 Å addressed nonbonding connections, whereas electrostatic forces were managed using the PME technique. The SHAKE algorithm restricted all bonds [23], while temperature and pressure were maintained stationary via the Berendsen weak coupling algorithm over the simulation [24]. Snapshots were taken through the trajectory at intervals of 10 ns for further investigations of each structure.

The PTRAJ and CPPTRAJ modules of AmberTools 14 were applied to analyze molecular dynamics trajectories of both the SHANK3 WT and the SHANK3 E71S mutant [23] of AmberTools 14. To evaluate the concurrent behavior of our structures, the RMSDs for SHANK3 WT and the SHANK3 E71S mutant have been analyzed, wherein the initial MD system was employed as the template for analysis.

Besides that, the two structures underwent Radius Gyration, hydrophobic interactions, and intramolecular distance analysis. The analysis of intra-molecular hydrogen bonds was performed for SHANK3 WT and the SHANK3 E71S mutant according to the potential donors (HD) and acceptors (HA) of the protons. UCSF Chimera software [19] was utilized to depict the 3D structure of each system. The Xmgrace plotting tools were applied to generate the plots. The monitoring of pressure, temperature, kinetic energy, total energy, and potential energy was systematically validated throughout the simulation time for the SHANK3 WT and the SHANK3 E71S mutant systems.

2.3. Docking between the two structures and αCaMKII analysis.

The docking between the two structures, SHANK3 WT and SHANK3 E71S mutant with protein partners αCaMKII and α-Fodrin, was conducted using a ClusPro (protein-protein docking) server, and the results were analyzed through the PDBsum server.

3. Results and Discussion

3.1. The root mean square deviation (RMSD).

RMSD analysis was carried out for a 200 ns simulation period comprising the SHANK3 WT protein and the SHANK3 E71S mutant. This analysis yielded crucial insights into their structural dynamics. RMSD of the SHANK3 WT protein exhibited a gradual rise with initial fluctuations, followed by a significant changeover at around 3.9 Å, and eventually stabilized towards the end of the simulation, as depicted in Figure 1a. Conversely, the SHANK3 E71S mutant demonstrated an abrupt increase in impulse at 4.5 Å, followed by a reduction in RMSD

and further fluctuations until the end of the simulation Figure 1c. The results indicate that the SHANK3 WT may exhibit greater stability than the SHANK3 E71S mutant, which could have increased structural flexibility. RMSD analyses were undertaken for the three domains SPN, ARR, and Linker individually to distinguish the domain that contributes to these conformational adjustments. RMSD analysis engaged to the SPN and ARR domains showed a consistent pattern with the SHANK3 WT protein, as exhibited in Figure 1b. In contrast, the SPN and ARR domains in the SHANK3 E71S mutant demonstrated greater fluctuations, suggesting their probable participation in constitutional alterations, as exhibited in Figure 1d.

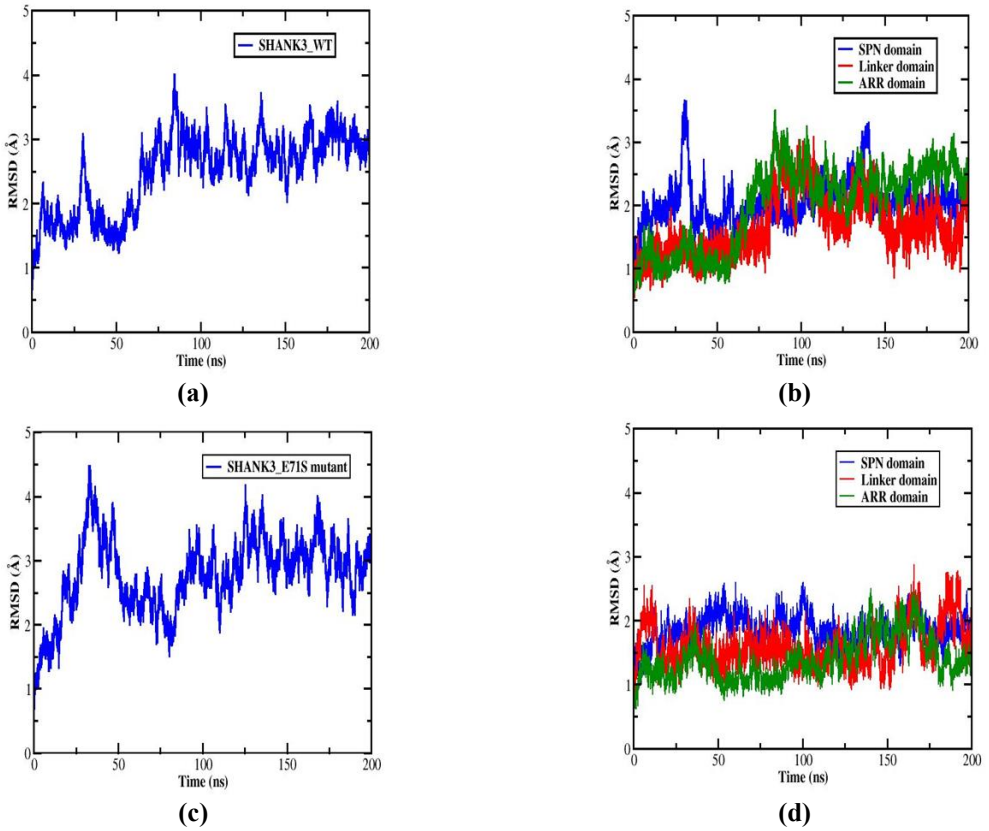

Figure 1. The MD simulation analysis RMSD plot for **(a)** SHANK3 WT; **(b)** Three domains in SHANK3 WT; **(c)** SHANK3 E71S mutant; **(d)** Three domains in SHANK3 E71S mutant. The RMSD values exhibited in Angstrom are shown on the y-axis, while the x-axis exhibits the time.

3.2. The root mean square fluctuation (RMSF).

The findings of RMSF indicated marginally higher conformational flexibility in the SHANK3 WT compared to the SHANK3 E71S mutant, as shown in Figures 2a and 2c, respectively. Noteworthy was the flexibility detected in amino acid residue corresponding to the position of the mutation of SHANK3 E71S mutant aligning with the SHANK3 SPN domain in the E71S mutant as exhibited in Figure 2d, shown to be higher than in the SHANK3 WT protein as illustrated in Figure 2b. The SPN domain with high RMSF values might be functionally important. The influence of the E71S mutant on SHANK3 folding has been studied by assessing the Rg indicator.

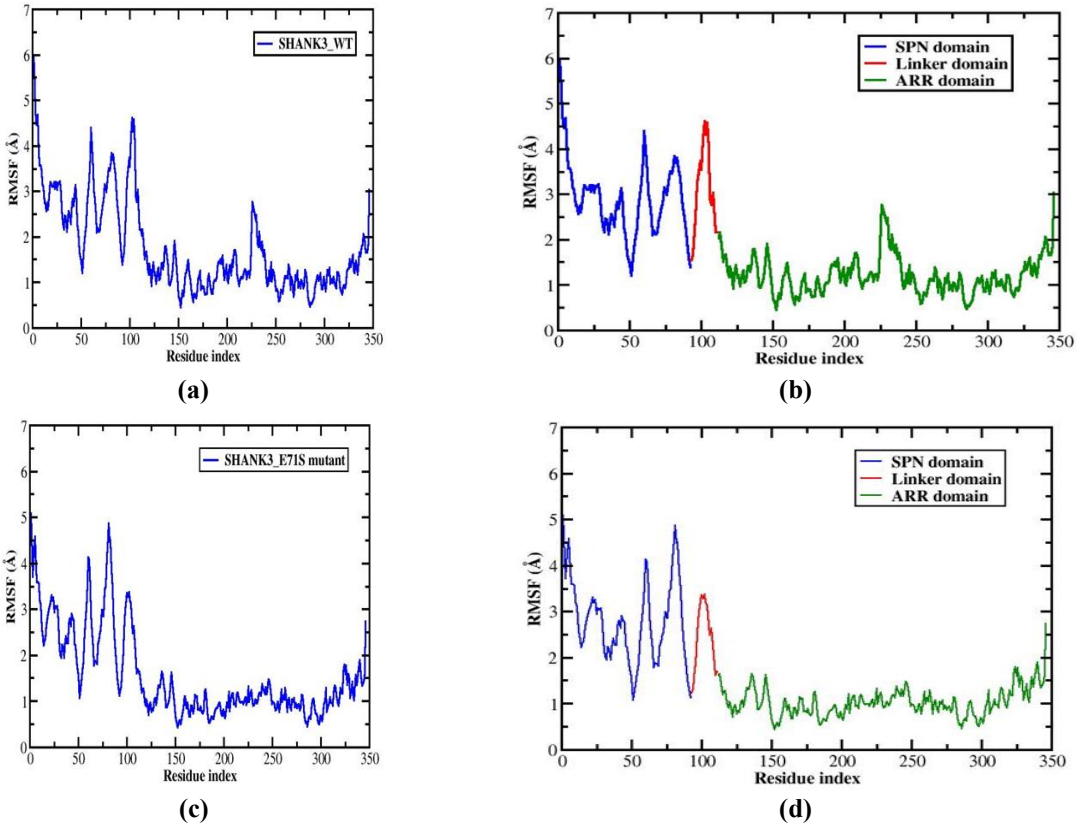

Figure 2. The MD simulation analysis RMSF plot for **(a)** SHANK3 WT; **(b)** Three domains in SHANK3 WT; **(c)** SHANK3 E71S mutant; **(d)** Three domains in SHANK3 E71S mutant. The RMSf values exhibits in Angstrom are shown on the y-axis, while the x-axis exhibits the residue index.

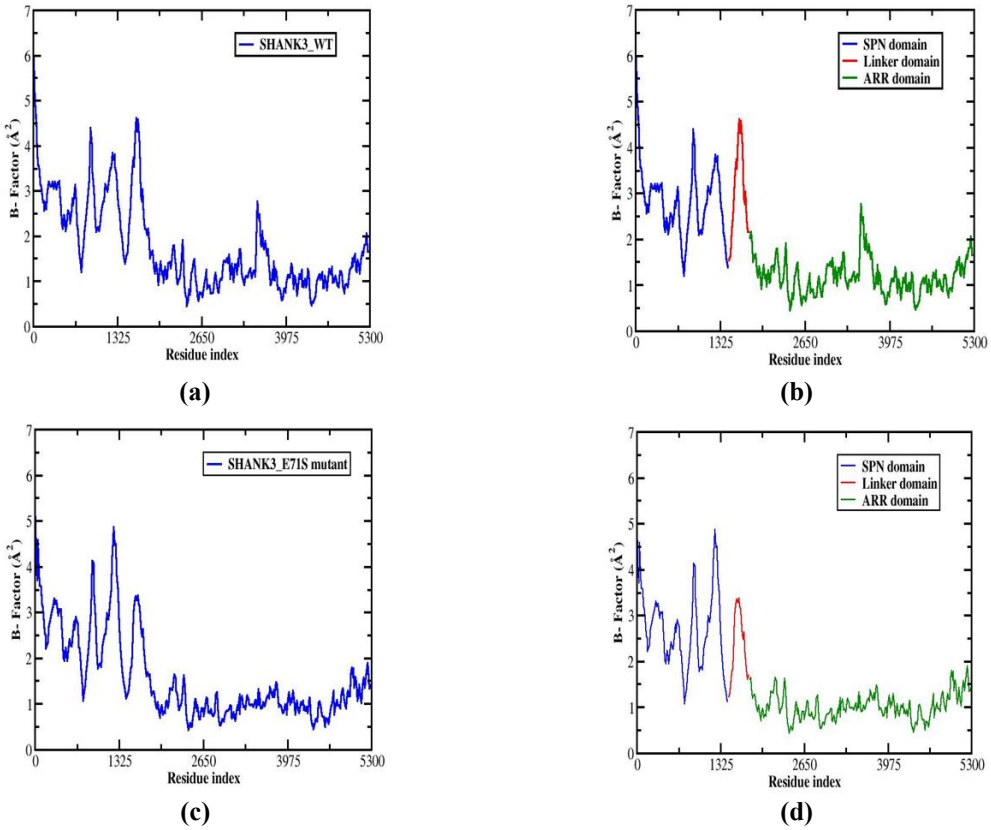

Figure 3. The MD simulation analysis B-Factor plot for **(a)** SHANK3 WT; **(b)** Three domains in SHANK3 WT; **(c)** SHANK3 E71S mutant; **(d)** Three domains in SHANK3 E71S mutant.

3.3. The B- Factor analysis.

The B-factor analysis evaluates the vibration of atoms in a molecular system through the time of the MD simulation, which furnishes perspectives on the spatial fluctuation of atoms around their equilibrium points. The SHANK3 WT protein demonstrated slightly heightened atomic flexibility than the SHANK3 E71S mutant, as depicted in Figures 3a and 3c, respectively. Strikingly, we noted further variations in the Cα atoms inside the portion harmonious to the mutation position in the SPN domain in the SHANK3 E71S mutant, as illustrated in Figure 3d, that displayed increased atomic motion and flexibility. However, the SHANK3 WT protein revealed lower values, as shown in Figure 3b, suggesting more stability.

3.4. The radius of gyration (Rg) analysis.

The radius of gyration (Rg) is a regularly adopted metric for evaluating the spatial distribution of atoms within a specific biological molecule computed from the principal center of gravity. The radius of gyration is applied to track changes in structural compactness and folded over simulation time. According to the Rg plots, the SHANK3 WT protein exposed lower values over time of the simulation of 200 ns, as exhibited in Figure 4a. Notably, the SHANK3 E71S mutant has elevated Rg values throughout the simulation, as shown in Figure 4b; therefore, the SHANK3 E71S mutant relates to a less compact and unfolded state. We apply the distance analysis between SPN and ARR domains to determine the constructional state between SPN and ARR domains.

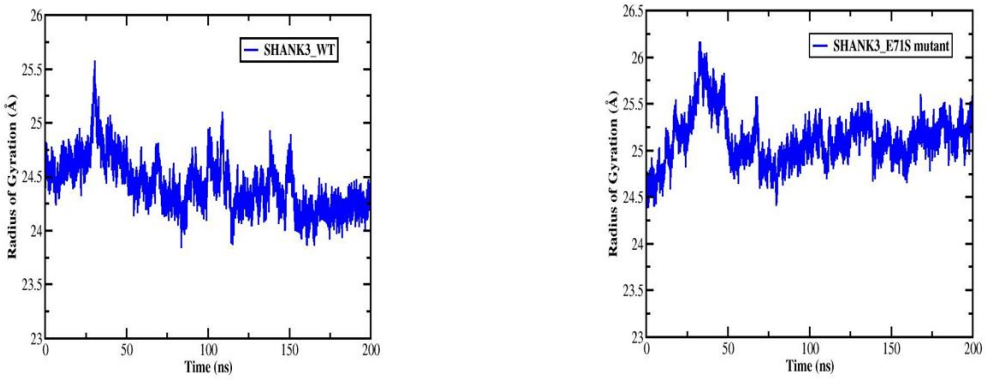

(a) **(b)**

Figure 4. The radius of gyration analysis Rg, **(a)** SHANK3 WT protein; **(b)** SHANK3 E71S mutant. The x-axis depicts the time ns, while the y-axis depicts the Radius gyration.

3.5. Analysis of the distance between SPN and ARR domains.

The central point of mass distance between the SPN-ARR domains of SHANK3 WT and the SHANK3 E71S mutant was evaluated. Initially, the distance between SPN-ARR in the SHANK3 WT protein increased, followed by a sudden reduction, and continued with a stabilization state to the end of the simulation, as exhibited in Figure 5a. Conversely, the SHANK3 E71Smutant exhibited a significant heightening in distance, then gradually decreased, followed by remarkable elevated compared to SHANK3 WT to the end of simulation time, reflecting an impact on domain interactions and the potential open-up of the SPN-ARR fold over time as shown in Figure 5b.

The loop structure between SPN and ARR serves as a specific site for the interaction with Ca^{2+}/calmodulin-dependent kinase IIα (CaMKIIα), which partially conceals the Ras binding site. Recent reports have pointed out the involvement of the linker domain in this loop

as a binding surface for αCaMKII. This binding arises in its inactive state, non-phosphorylated, and requires a closed configuration of the SPN-ARR tandem [17, 25]. Consequently, disrupting the connections between SPN and ARR regions may induce a conformational alteration in the Linker domain, leading to lower affinity to αCaMKII. Our findings corresponded with previous results and revealed that the interaction between the SHANK3 WT protein and αCaMKII displayed higher interactions, as indicated in Table S1, Figures S1(A) and S2(A) compared to the interactions reported in the SHANK3 E71S mutant with αCaMKII, as depicted in Table S2, Figures S1(B) and S2(B). However, the distinctive interaction between αCaMKII and SHANK3 plays a pivotal role in instigating a specialized long-range signaling pathway from the plasma cell membrane, specifically L-type calcium channels (LTCCs), to the nucleus. This signaling mechanism is imperative for inducing activity-dependent alterations in neuronal gene transcription during memory and learning processes [26]. It was claimed the disruption of αCaMKII activity emerges as a prevalent process, generating modifications to the structure of glutamatergic and plasticity neuron function, contributing to the pathogenesis of neurological disorders, including autism [27]. In addition, CaMKIIα is a crucial element in synaptic plasticity and learning mechanisms that play an important role in processing synaptic Ca^{2+} fluctuations, regulating calcium levels, PSD integration, and shaping the morphology of dendritic spines [25].

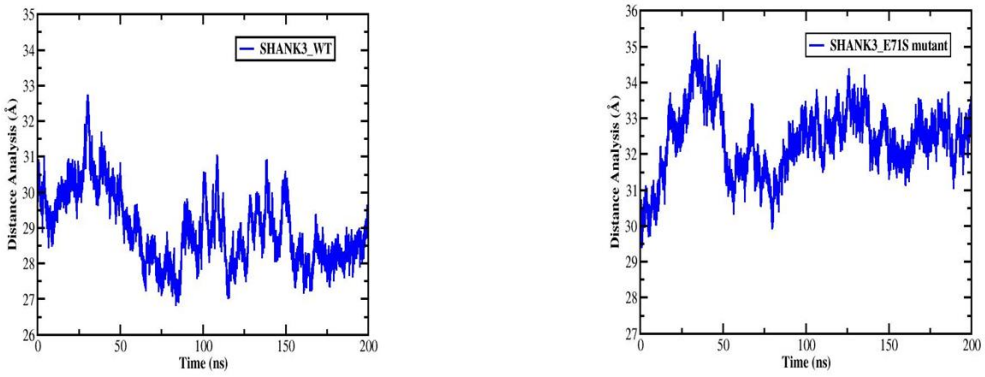

(a) **(b)**

Figure 5. The distance between SPN and ARR domains analysis, **(a)** SHANK3 WT protein; **(b)** SHANK3 E71S mutant.

3.6. Intra-molecular hydrogen bond analysis.

Intramolecular hydrogen bonds were assessed to gauge the proximity of all-atom interactions within the SHANK3 WT protein and SHANK3 E71S mutant. These intramolecular hydrogen bond contacts are relevant indicators used for measuring the structural compactness within the distinct domains of the SHANK3 WT protein. Figures 6a and 7a, respectively, show that the SHANK3 WT protein, as shown in Table S5 had more intramolecular interactions than the SHANK3 E71S mutant. Similar differences were seen in the SPN domain between the SHANK3 WT protein (Figure 6b) and the SHANK3 E71S mutant (Figure 7b). Moreover, Figures 6c and 6d of the SHANK3 WT protein and Figures 7c and 7d of the SHANK3 E71S mutant did not exhibit any appreciable variations in the ARR and Linker domains. According to our findings, the SHANK3 WT protein exhibits high molecular interactions within the SPN, which are linked to the protein's overall stability and maintenance of a closed conformation, as previously seen in Figure 3a. On the other hand, as Figure 5b illustrates, the SHANK3 E71S mutant significantly increased the distance between the SPN and ARR regions by disrupting the intramolecular connections between SPN and ARR. The

functional significance of the intramolecular connections between SPN and ARR in SHANK3 [28] and their implications in the pathophysiology of ASD have been the subject of numerous investigations.

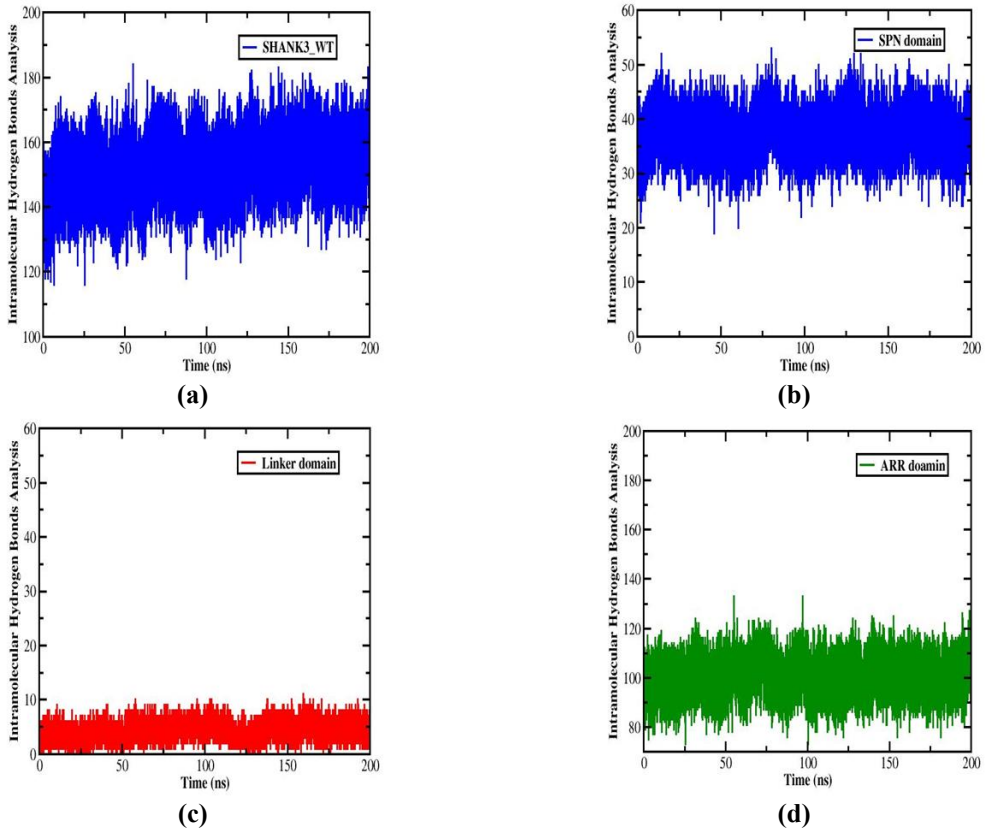

Figure 6. The intramolecular hydrogen bonds analysis, **(a)** SHANK3 WT protein; **(b)** SPN domain of SHANK3 WT; **(c)** Linker domain of SHANK3 WT; **(d)** ARR domain of SHANK3 WT.

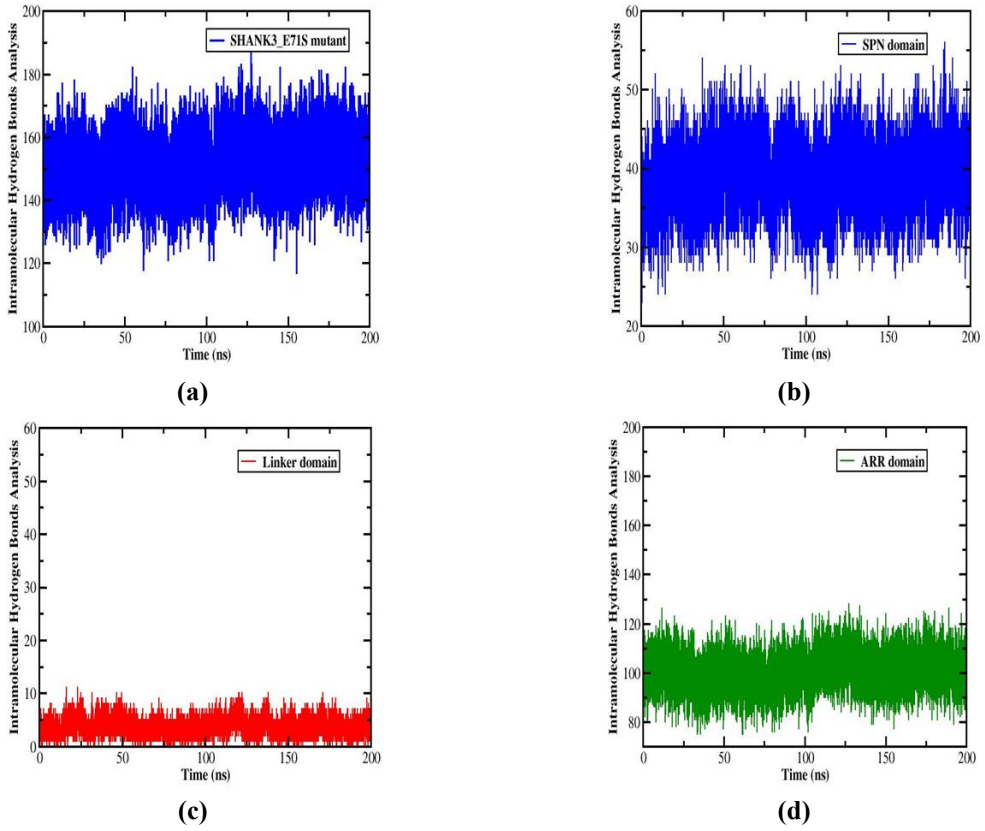

Figure 7. The intramolecular hydrogen bonds analysis, **(a)** SHANK3 E71S mutant; **(b)** SPN domain of SHANK3 E71S; **(c)** Linker domain of SHANK3 E71S; **(d)** ARR domain of SHANK3 E71S.

Previous studies revealed that α-Fodrin cannot reach its position on the ARR domain in SHANK3 WT due to intramolecular interaction [29]. At the same time, the α-Fodrin connection to SHANK3 was greatly enhanced in the SHANK3 P141A mutant due to the disruption of SPN and ARR domain connections [17]. Our findings showed that the SHANK3 E71S mutant interfered with the interactions between SPN-ARR domains., so the potential scenario might be that the SHANK3 E71S mutant opens the conformation and facilitates α-Fodrin binding, which increases actin linkage and enhances integrin activation. Taken together, this mutant might change the flexible conformation of SHANK3, impairing the capacity to coordinate cytoskeletal aggregation and signaling dysregulation. The physiological activity of the SHANK3-actin connection influences dendritic protrusion morphology in neuron cells and ASD-related characteristics in vivo [16]. Our findings align with the previous study that SHANK3 WT showed lower interactions with α-Fodrin Figures S3(A) and S4(A) as well as Table S3 in comparison with SHANK3 E71S mutant as depicted in Figures S3(B) and S4(B), as well as Table S4.

3.7. Hydrogen bond analysis.

The interaction between the SPN and ARR domains was studied through hydrogen bonds. A 200 ns simulation was undertaken for both the SHANK3 WT protein and the SHANK3 E71S mutant to spotlight the specificity of this interaction, a critical aspect of molecular recognition. The analysis targeted residues aa1-92 for the SPN domain and residues aa112-346 for the ARR domain. The findings indicated that the SHANK3 WT protein exhibited more hydrogen bonds than the SHANK3 E71S mutant, as shown in Figures 8a and 8b, indicating more stability.

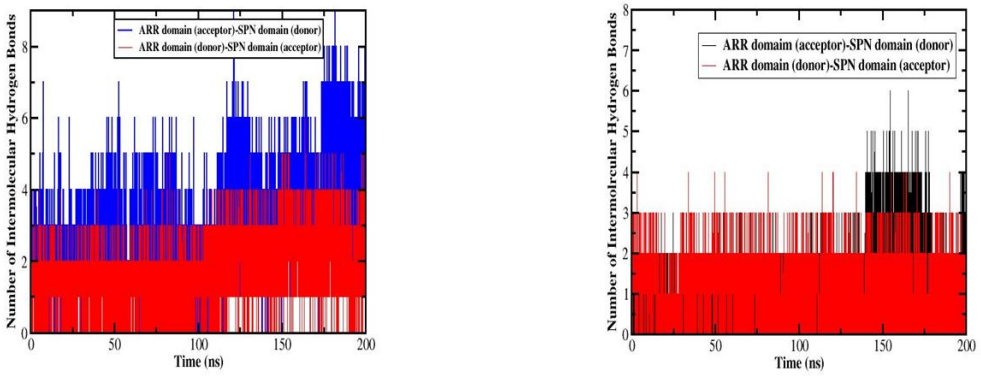

(a) **(b)**

Figure 8. Number of hydrogen bonds between SPN and ARR for 200 ns trajectory, **(a)** SHANK3 WT protein; **(b)** SHANK3 E71S mutant.

3.8. Secondary structure analysis.

The secondary structure analysis of the two structures, the SHANK3 WT protein, and the SHANK3 E71S mutant were applied. The plots depicting the outcomes for the secondary structure analysis for the SHANK3 WT protein are presented in Figures 9a-d and the SHANK3 E71S mutant, as shown in Figures 10a-d. The graphics illustrate the variability of secondary structure across each residue as an indication of frame numbers. We conducted an assessment of the secondary structure probability assumed by the SHANK3 WT and SHANK3 E71S mutant, employing quantitative measures as a function of residue index, as delineated in

Figures 11a-d for SHANK3 WT protein, and for SHANK3 E71S mutant as shown in Figures 12a-d.

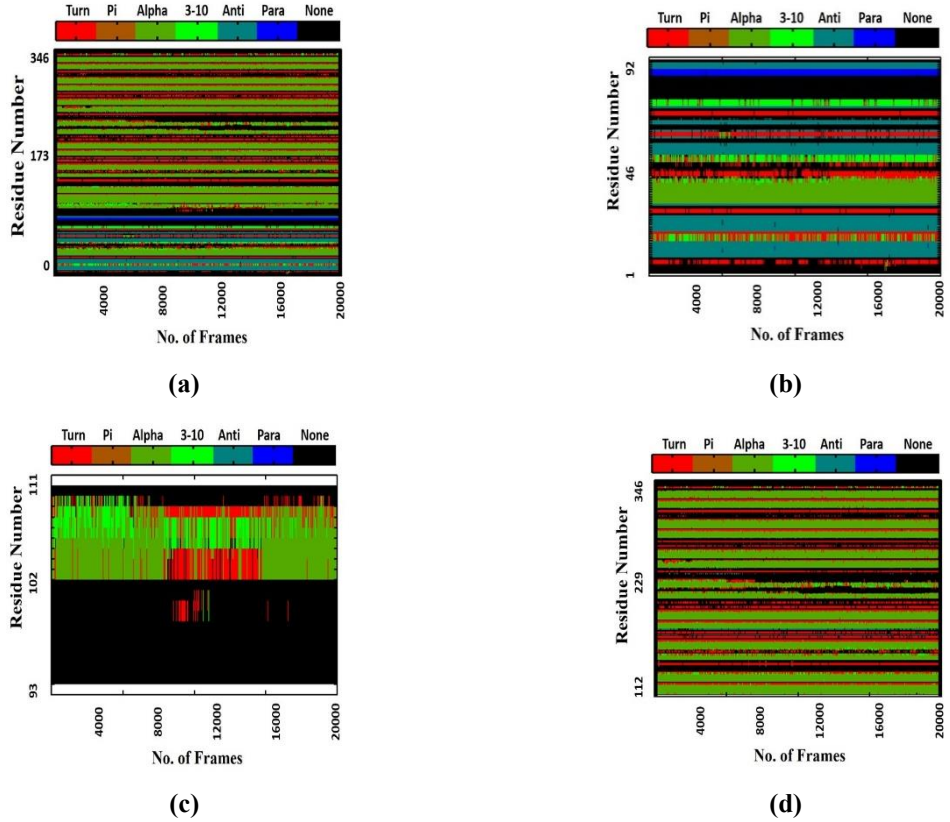

Figure 9. The analysis of secondary structure, **(a)** SHANK3 WT protein; **(b)** SPN domain; **(c)** Linker domain; **(d)** and ARR domain.

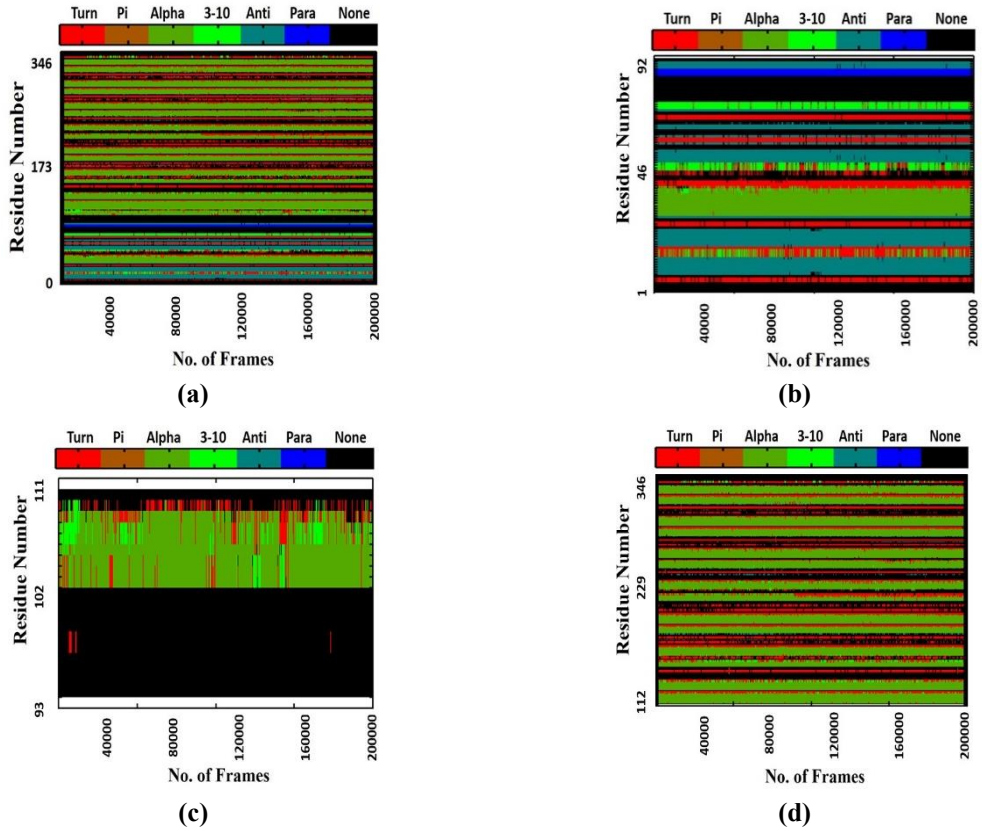

Figure 10. The analysis of secondary structure **(a)** SHANK3 E71S mutant; **(b)** SPN region; **(c)** Linker region; **(d)** and ARR region.

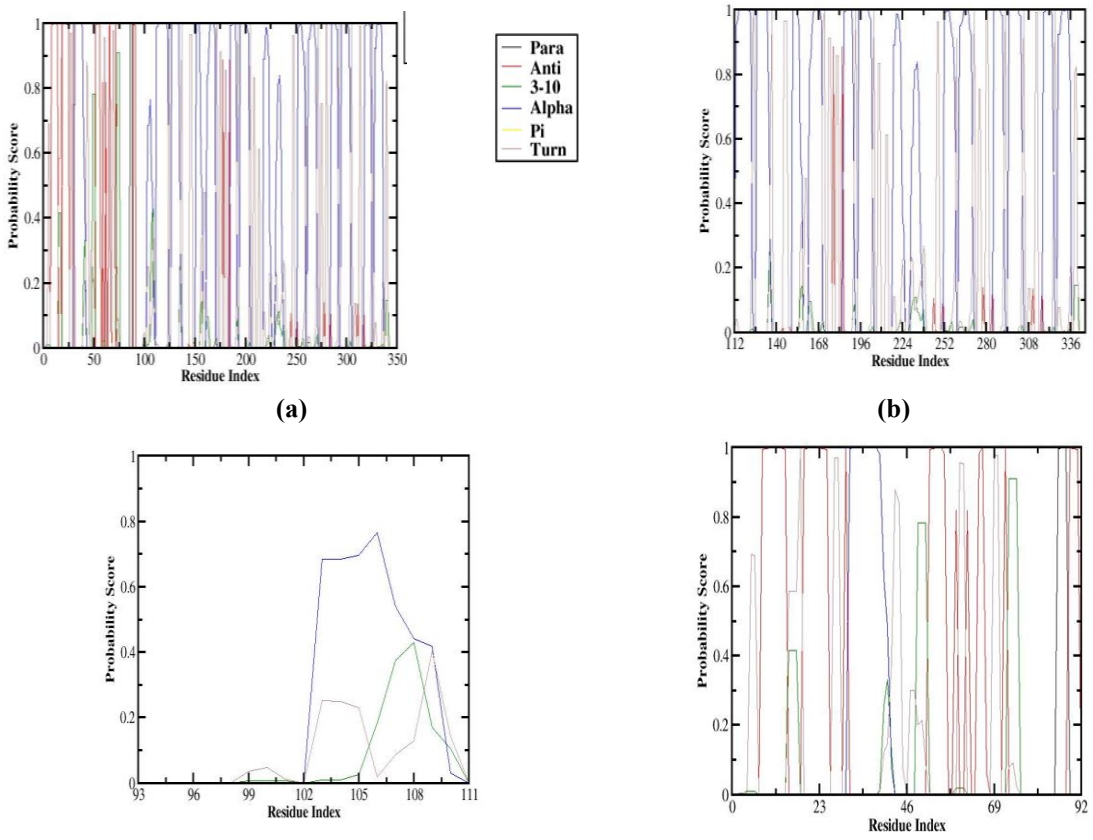

Figure 11. The secondary structure probability score of residue index: **(a)** SHANK3 WT protein; **(b)** SPN region; **(c)** Linker region; **(d)** and ARR region.

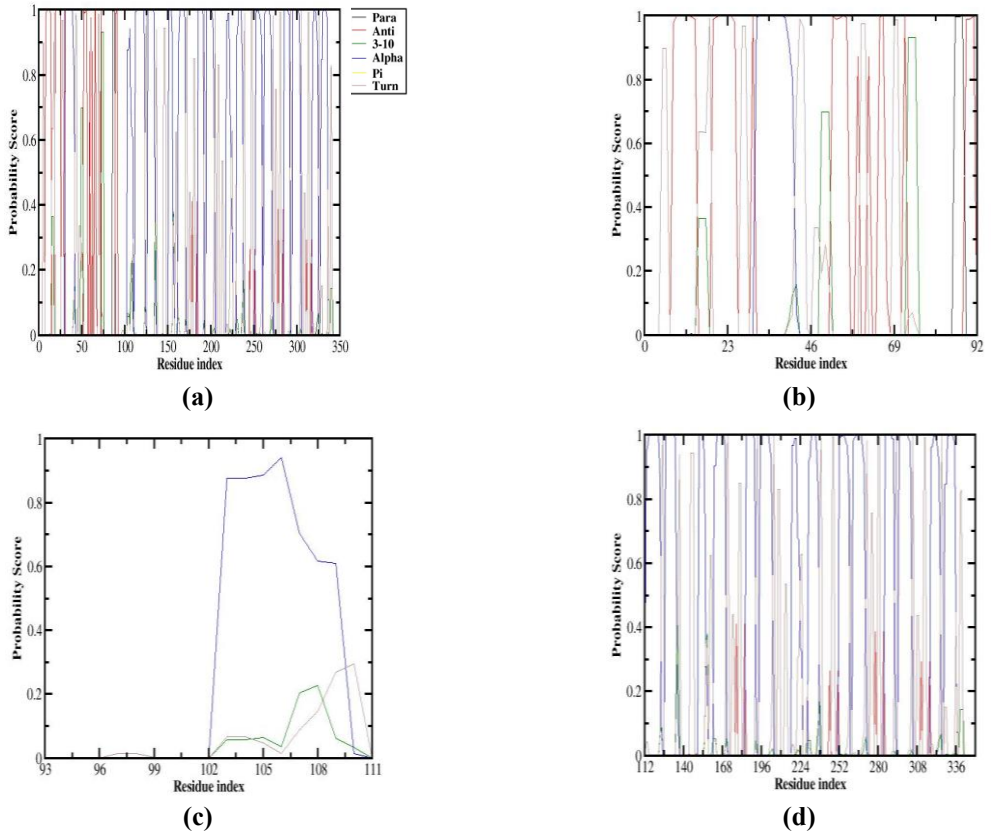

Figure 12. The secondary structure probability score of residue index: **(a)** SHANK3 E71S mutant; **(b)** SPN region; **(c)** Linker region; **(d)** and ARR region.

4. Conclusions

In conclusion, we thoroughly examined the consequences of the SHANK3 E71S mutant, which is found in the SHANK3 gene's N-terminal region. The study found Important ramifications, most notably that it hindered the SHANK3 protein's folding and stabilization processes. The disruption of intramolecular interactions between the SPN and ARR domains by the SHANK3 E71S mutant positively impacted its binding with αCaMKII. It is expected that this disruption will have a major effect on synaptic functioning and may even play a role in the pathophysiology of ASD. In contrast, α-Fodrin's binding affinity to its site on the ARR domain was reduced due to the SHANK3 E71S mutation. The complex dynamics of SHANK3 mutations, which lead to modified configurations, highlight their possible involvement in neurodevelopmental conditions like autism spectrum disorders. To clarify the precise contributions of this type of mutation to the pathophysiology of ASD, more computational and experimental research is necessary.

Funding

This research received no external funding.

Acknowledgments

The authors acknowledge Tezpur University and the Indian Council for Cultural Relations (ICCR) for their support.

Conflicts of Interest

The authors declare no conflict of interest.

References

1. Nisar, S.; Haris, M. Neuroimaging genetics approaches to identify new biomarkers for the early diagnosis of autism spectrum disorder. *Mol. Psychiatry* **2023**, *28*, 4995-5008, https://doi.org/10.1038/s41380-023-02060-9.
2. Zeidan, J.; Fombonne, E.; Scorah, J.; Ibrahim, A.; Durkin, M.S.; Saxena, S.; Yusuf, A.; Shih, A.; Elsabbagh, M. Global prevalence of autism: A systematic review update. *Autism Res.* **2022,** *15*, 778-790, https://doi.org/10.1002/aur.2696.
3. Ghafouri-Fard, S.; Pourtavakoli, A.; Hussen, B.M.; Taheri, M.; Ayatollahi, S.A. A Review on the Role of Genetic Mutations in the Autism Spectrum Disorder. *Mol. Neurobiol.* **2023**, *60*, 5256–5272, https://doi.org/10.1007/s12035-023-03405-9.
4. Molloy, C.J.; Cooke, J.; Gatford, N.J.F.; Rivera-Olvera, A.; Avazzadeh, S.; Homberg, J.R.; Grandjean, J.; Fernandes, C.; Shen, S.; Loth, E.; Srivastava, D.P.; Gallagher, L. Bridging the translational gap: what can synaptopathies tell us about autism?. *Front. Mol. Neurosci.* **2023**, *16*, 1191323, https://doi.org/10.3389/fnmol.2023.1191323.
5. Monteiro, P.; Feng, G. SHANK proteins: roles at the synapse and in autism spectrum disorder. *Nat. Rev. Neurosci.* **2017**, *18*, 147-157, https://doi.org/10.1038/nrn.2016.183.
6. Satterstrom, F.K.; Kosmicki, J.A.; Wang, J.; Breen, M.S.; De Rubeis, S.; An, J.-Y.; Peng, M.; Collins, R.; Grove, J.; Klei, L.; Stevens, C.; Reichert, J.; Mulhern, M.S.; Artomov, M.; Gerges, S.; Sheppard, B.; Xu, X.; Bhaduri, A.; Norman, U.; Brand, H.; Schwartz, G.; Nguyen, R.; Guerrero, E.E.; Dias, C.; Aleksic, B.; Anney, R.; Barbosa, M.; Bishop, S.; Brusco, A.; Bybjerg-Grauholm, J.; Carracedo, A.; Chan, M.C.Y.; Chiocchetti, A.G.; Chung, B.H.Y.; Coon, H.; Cuccaro, M.L.; Curró, A.; Dalla Bernardina, B.; Doan, R.; Domenici, E.; Dong, S.; Fallerini, C.; Fernández-Prieto, M.; Ferrero, G.B.; Freitag, C.M.; Fromer, M.; Gargus, J.J.; Geschwind, D.; Giorgio, E.; González-Peñas, J.; Guter, S.; Halpern, D.; Hansen-Kiss, E.; He, X.; Herman, G.E.; Hertz-Picciotto, I.; Hougaard, D.M.; Hultman, C.M.; Ionita-Laza, I.; Jacob, S.; Jamison, J.; Jugessur,

A.; Kaartinen, M.; Knudsen, G.P.; Kolevzon, A.; Kushima, I.; Lee, S.L.; Lehtimäki, T.; Lim, E.T.; Lintas, C.; Lipkin, W.I.; Lopergolo, D.; Lopes, F.; Ludena, Y.; Maciel, P.; Magnus, P.; Mahjani, B.; Maltman, N.; Manoach, D.S.; Meiri, G.; Menashe, I.; Miller, J.; Minshew, N.; Montenegro, E.M.S.; Moreira, D.; Morrow, E.M.; Mors, O.; Mortensen, P.B.; Mosconi, M.; Muglia, P.; Neale, B.M.; Nordentoft, M.; Ozaki, N.; Palotie, A.; Parellada, M.; Passos-Bueno, M.R.; Pericak-Vance, M.; Persico, A.M.; Pessah, I.; Puura, K.; et al. Large-Scale Exome Sequencing Study Implicates Both Developmental and Functional Changes in the Neurobiology of Autism. *Cell* **2020**, *180*, 568-584.e23, https://doi.org/10.1016/j.cell.2019.12.036.

7. Fu, J.M.; Satterstrom, F.K.; Peng, M.; Brand, H.; Collins, R.L.; Dong, S.; Wamsley, B.; Klei, L.; Wang, L.; Hao, S.P.; Stevens, C.R.; Cusick, C.; Babadi, M.; Banks, E.; Collins, B.; Dodge, S.; Gabriel, S.B.; Gauthier, L.; Lee, S.K.; Liang, L.; Ljungdahl, A.; Mahjani, B.; Sloofman, L.; Smirnov, A.N.; Barbosa, M.; Betancur, C.; Brusco, A.; Chung, B.H.Y.; Cook, E.H.; Cuccaro, M.L.; Domenici, E.; Ferrero, G.B.; Gargus, J.J.; Herman, G.E.; Hertz-Picciotto, I.; Maciel, P.; Manoach, D.S.; Passos-Bueno, M.R.; Persico, A.M.; Renieri, A.; Sutcliffe, J.S.; Tassone, F.; Trabetti, E.; Campos, G.; Cardaropoli, S.; Carli, D.; Chan, M.C.Y.; Fallerini, C.; Giorgio, E.; Girardi, A.C.; Hansen-Kiss, E.; Lee, S.L.; Lintas, C.; Ludena, Y.; Nguyen, R.; Pavinato, L.; Pericak-Vance, M.; Pessah, I.N.; Schmidt, R.J.; Smith, M.; Costa, C.I.S.; Trajkova, S.; Wang, J.Y.T.; Yu, M.H.C.; Aleksic, B.; Artomov, M.; Benetti, E.; Biscaldi-Schafer, M.; Børglum, A.D.; Carracedo, A.; Chiocchetti, A.G.; Coon, H.; Doan, R.N.; Fernández-Prieto, M.; Freitag, C.M.; Gerges, S.; Guter, S.; Hougaard, D.M.; Hultman, C.M.; Jacob, S.; Kaartinen, M.; Kolevzon, A.; Kushima, I.; Lehtimäki, T.; Rizzo, C.L.; Maltman, N.; Manara, M.; Meiri, G.; Menashe, I.; Miller, J.; Minshew, N.; Mosconi, M.; Ozaki, N.; Palotie, A.; Parellada, M.; Puura, K.; Reichenberg, A.; Sandin, S.; Scherer, S.W.; Schlitt, S.; et al. Rare coding variation provides insight into the genetic architecture and phenotypic context of autism. *Nat. Genet.* **2022**, *54*, 1320-1331, https://doi.org/10.1038/s41588-022-01104-0.
8. Zhou, X.; Feliciano, P.; Shu, C.; Wang, T.; Astrovskaya, I.; Hall, J.B.; Obiajulu, J.U.; Wright, J.R.; Murali, S.C.; Xu, S.X.; Brueggeman, L.; Thomas, T.R.; Marchenko, O.; Fleisch, C.; Barns, S.D.; Snyder, L.G.; Han, B.; Chang, T.S.; Turner, T.N.; Harvey, W.T.; Nishida, A.; O'Roak, B.J.; Geschwind, D.H.; Adams, A.; Amatya, A.; Andrus, A.; Bashar, A.; Berman, A.; Brown, A.; Camba, A.; Gulsrud, A.C.; Krentz, A.D.; Shocklee, A.D.; Esler, A.; Lash, A.E.; Fanta, A.; Fatemi, A.; Fish, A.; Goler, A.; Gonzalez, A.; Gutierrez, A.; Hardan, A.; Hess, A.; Hirshman, A.; Holbrook, A.; Ace, A.J.; Griswold, A.J.; Gruber, A.J.; Jarratt, A.; Jelinek, A.; Jorgenson, A.; Juarez, A.P.; Kim, A.; Kitaygorodsky, A.; Luo, A.; Rachubinski, A.L.; Wainer, A.L.; Daniels, A.M.; Mankar, A.; Mason, A.; Miceli, A.; Milliken, A.; Morales-Lara, A.; Stephens, A.N.; Nguyen, A.N.; Nicholson, A.; Paolicelli, A.M.; McKenzie, A.P.; Gupta, A.R.; Raven, A.; Rhea, A.; Simon, A.; Soucy, A.; Swanson, A.; Sziklay, A.; Tallbull, A.; Tesng, A.; Ward, A.; Zick, A.; Hilscher, B.A.; Bell, B.; Enright, B.; Robertson, B.E.; Hauf, B.; Jensen, B.; Lobisi, B.; Vernoia, B.M.; Schwind, B.; VanMetre, B.; Erickson, C.A.; Sullivan, C.A.W.; Albright, C.; Anglo, C.; Buescher, C.; Bradley, C.C.; Campo-Soria, C.; Cohen, C.; Colombi, C.; Diggins, C.; Edmonson, C.; et al. Integrating de novo and inherited variants in 42,607 autism cases identifies mutations in new moderate-risk genes. *Nat. Genet.* **2022**, *54*, 1305-1319, https://doi.org/10.1038/s41588-022-01148-2.
9. Cai, Q.; Hosokawa, T.; Zeng, M.; Hayashi, Y.; Zhang, M. Shank3 Binds to and Stabilizes the Active Form of Rap1 and HRas GTPases via Its NTD-ANK Tandem with Distinct Mechanisms. *Structure* **2020**, *28*, 290-300.e4, https://doi.org/10.1016/j.str.2019.11.018.
10. Hassani Nia, F.; Woike, D.; Martens, V.; Klüssendorf, M.; Hönck, H.-H.; Harder, S.; Kreienkamp, H.-J. Targeting of δ-catenin to postsynaptic sites through interaction with the Shank3 N-terminus. *Mol. Autism* **2020**, *11*, 85, https://doi.org/10.1186/s13229-020-00385-8.
11. Chiu, S.-L.; Chen, C.-M.; Huganir, R.L. ICA69 regulates activity-dependent synaptic strengthening and learning and memory. *Front. Mol. Neurosci.* **2023**, *16*, 1171432, https://doi.org/10.3389/fnmol.2023.1171432.
12. MacGillavry, H.D.; Kerr, J.M.; Kassner, J.; Frost, N.A.; Blanpied, T.A. Shank–cortactin interactions control actin dynamics to maintain flexibility of neuronal spines and synapses. *Eur. J. Neurosci.* **2016**, *43*, 179-193, https://doi.org/10.1111/ejn.13129.
13. Hassani Nia, F.; Kreienkamp, H.-J. Functional Relevance of Missense Mutations Affecting the N-Terminal Part of Shank3 Found in Autistic Patients. *Front. Mol. Neurosci.* **2018**, *11*, 00268, https://doi.org/10.3389/fnmol.2018.00268.
14. Durand, C.M.; Betancur, C.; Boeckers, T.M.; Bockmann, J.; Chaste, P.; Fauchereau, F.; Nygren, G.; Rastam, M.; Gillberg, I.C.; Anckarsäter, H.; Sponheim, E.; Goubran-Botros, H.; Delorme, R.; Chabane, N.; Mouren-Simeoni, M.-C.; de Mas, P.; Bieth, E.; Rogé, B.; Héron, D.; Burglen, L.; Gillberg, C.; Leboyer, M.;

Bourgeron, T. Mutations in the gene encoding the synaptic scaffolding protein SHANK3 are associated with autism spectrum disorders. *Nat. Genet.* **2007**, *39*, 25-27, https://doi.org/10.1038/ng1933.
15. Lilja, J.; Zacharchenko, T.; Georgiadou, M.; Jacquemet, G.; Franceschi, Nicola D.; Peuhu, E.; Hamidi, H.; Pouwels, J.; Martens, V.; Nia, Fatemeh H.; Beifuss, M.; Boeckers, T.; Kreienkamp, H.-J.; Barsukov, Igor L.; Ivaska, J. SHANK proteins limit integrin activation by directly interacting with Rap1 and R-Ras. *Nat. Cell Biol.* **2017**, *19*, 292-305, https://doi.org/10.1038/ncb3487.
16. Salomaa, S.I.; Miihkinen, M.; Kremneva, E.; Paatero, I.; Lilja, J.; Jacquemet, G.; Vuorio, J.; Antenucci, L.; Kogan, K.; Hassani Nia, F.; Hollos, P.; Isomursu, A.; Vattulainen, I.; Coffey, E.T.; Kreienkamp, H.-J.; Lappalainen, P.; Ivaska, J. SHANK3 conformation regulates direct actin binding and crosstalk with Rap1 signaling. *Curr. Biol.* **2021**, *31*, 4956-4970.e9, https://doi.org/10.1016/j.cub.2021.09.022.
17. Woike, D.; Wang, E.; Tibbe, D.; Hassani Nia, F.; Failla, A.V.; Kibæk, M.; Overgård, T.M.; Larsen, M.J.; Fagerberg, C.R.; Barsukov, I.; Kreienkamp, H.-J. Mutations affecting the N-terminal domains of SHANK3 point to different pathomechanisms in neurodevelopmental disorders. *Sci. Rep.* **2022**, *12*, 902, https://doi.org/10.1038/s41598-021-04723-5.
18. Berman, H.M.; Westbrook, J.; Feng, Z.; Gilliland, G.; Bhat, T.N.; Weissig, H.; Shindyalov, I.N.; Bourne, P.E. The Protein Data Bank. *Nucleic Acids Res.* **2000**, *28*, 235-242, https://doi.org/10.1093/nar/28.1.235.
19. Pettersen, E.F.; Goddard, T.D.; Huang, C.C.; Couch, G.S.; Greenblatt, D.M.; Meng, E.C.; Ferrin, T.E. UCSF Chimera—A visualization system for exploratory research and analysis. *J. Comput. Chem.* **2004**, *25*, 1605-1612, https://doi.org/10.1002/jcc.20084.
20. Henriques, J.; Cragnell, C.; Skepö, M. Molecular Dynamics Simulations of Intrinsically Disordered Proteins: Force Field Evaluation and Comparison with Experiment. *J. Chem. Theory Comput.* **2015**, *11*, 3420-3431, https://doi.org/10.1021/ct501178z.
21. Jorgensen, W.L.; Chandrasekhar, J.; Madura, J.D.; Impey, R.W.; Klein, M.L. Comparison of simple potential functions for simulating liquid water. *J. Chem. Phys.* **1983**, *79*, 926-935, https://doi.org/10.1063/1.445869.
22. Salomon-Ferrer, R.; Götz, A.W.; Poole, D.; Le Grand, S.; Walker, R.C. Routine Microsecond Molecular Dynamics Simulations with AMBER on GPUs. 2. Explicit Solvent Particle Mesh Ewald. *J. Chem. Theory Comput.* **2013**, *9*, 3878-3888, https://doi.org/10.1021/ct400314y.
23. Ryckaert, J.-P.; Ciccotti, G.; Berendsen, H.J.C. Numerical integration of the cartesian equations of motion of a system with constraints: molecular dynamics of *n*-alkanes. *J. Comput. Phys.* **1977**, *23*, 327-341, https://doi.org/10.1016/0021-9991(77)90098-5.
24. Berendsen, H.J.C.; Postma, J.P.M.; van Gunsteren, W. F.; DiNola, A.; Haak, J.R. Molecular dynamics with coupling to an external bath. *J. Chem. Phys.* **1984**, *81*, 3684-3690, https://doi.org/10.1063/1.448118.
25. Cai, Q.; Zeng, M.; Wu, X.; Wu, H.; Zhan, Y.; Tian, R.; Zhang, M. CaMKIIα-driven, phosphatase-checked post-synaptic plasticity via phase separation. *Cell Res.* **2021**, *31*, 37-51, https://doi.org/10.1038/s41422-020-00439-9.
26. Perfitt, T.L.; Wang, X.; Dickerson, M.T.; Stephenson, J.R.; Nakagawa, T.; Jacobson, D.A.; Colbran, R.J. Neuronal L-type calcium channel signaling to the nucleus requires a novel CaMKIIα-Shank3 interaction. *J. Neurosci.* **2020**, *40*, 2000-2014, https://doi.org/10.1523/JNEUROSCI.0893-19.2020.
27. Robison, A.J. Emerging role of CaMKII in neuropsychiatric disease. *Trends Neurosci.* **2014**, *37*, 653-662, https://doi.org/10.1016/j.tins.2014.07.001.
28. Woike, D.; Tibbe, D.; Nia, F.H.; Martens, V.; Wang, E.; Barsukov, I.; Kreienkamp, H.-J. The Shank/ProSAP N-terminal (SPN) domain of Shank3 regulates targeting to post-synaptic sites and post-synaptic signalling. *bioRxiv* **2023**, 2023.2004.2028.538665, https://doi.org/10.1101/2023.04.28.538665.
29. Mameza, M.G.; Dvoretskova, E.; Bamann, M.; Hönck, H.-H.; Güler, T.; Boeckers, T.M.; Schoen, M.; Verpelli, C.; Sala, C.; Barsukov, I.; Dityatev, A.; Kreienkamp, H.-J. SHANK3 Gene Mutations Associated with Autism Facilitate Ligand Binding to the Shank3 Ankyrin Repeat Region. *J. Biol. Chem.* **2013**, *288*, 26697-26708, https://doi.org/10.1074/jbc.M112.424747.

Supplementary materials

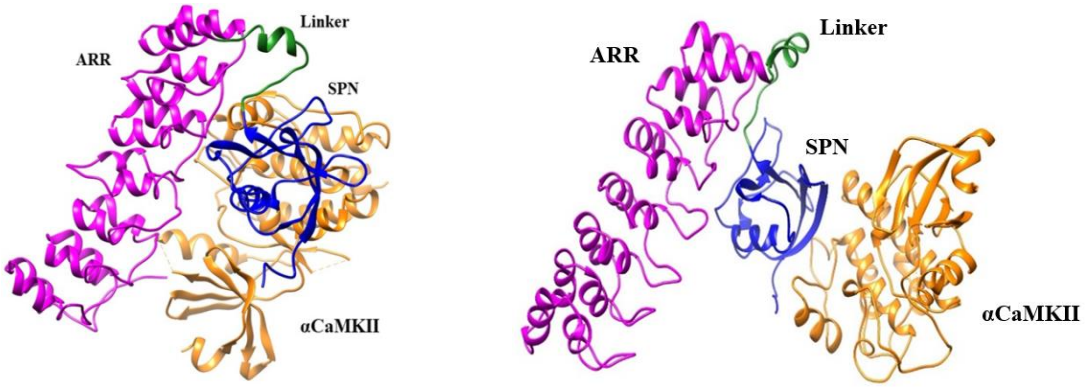

(A) **(B)**

Figure S1. The docking interaction between **(A)** SHANK3 WT protein and αCaMKII; **(B)** SHANK3 E71S mutant and αCaMKII.

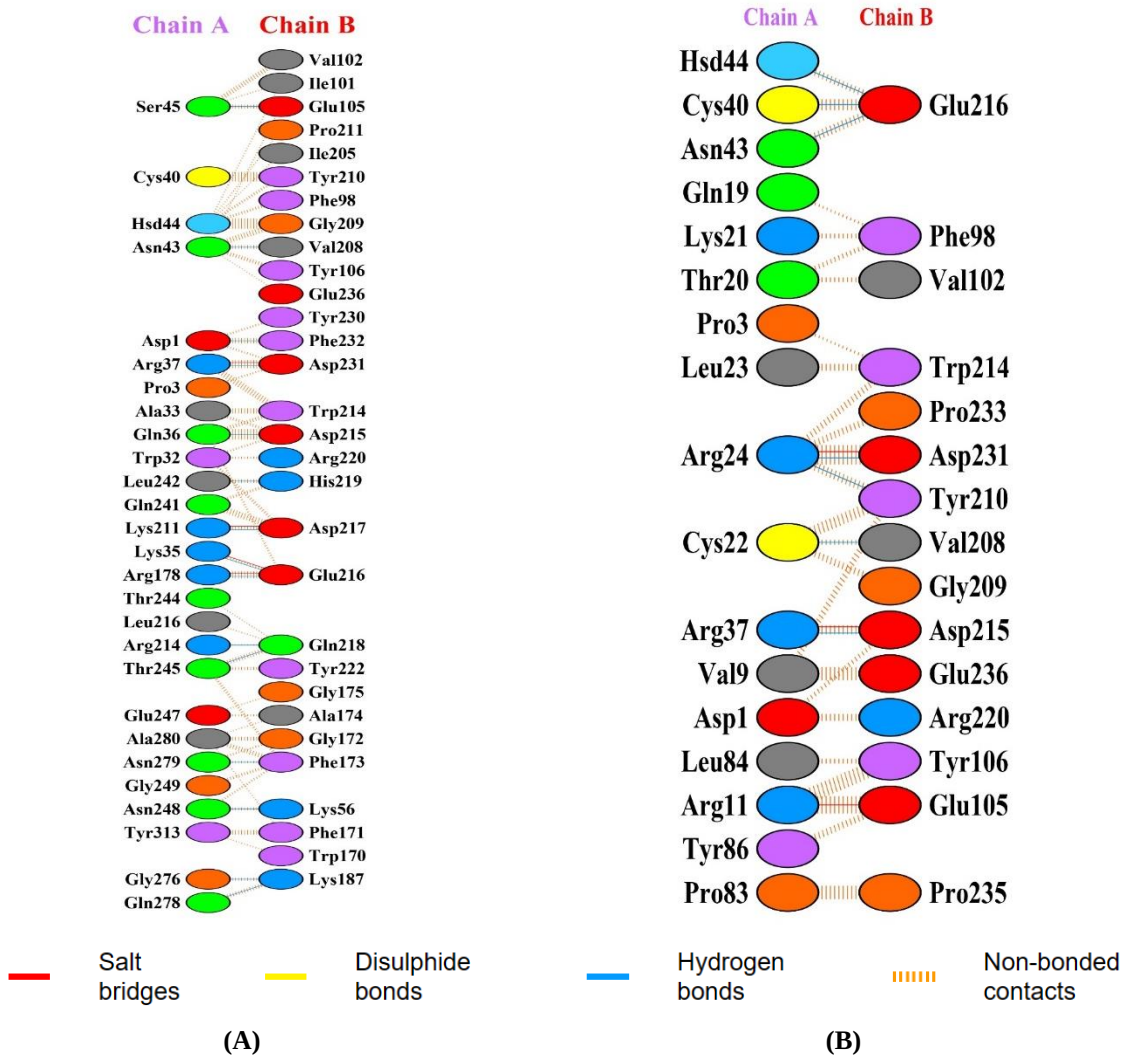

(A) **(B)**

Figure S2. The interactions between **(A)** SHANK3 WT protein (chain A) with αCaMKII (chain B); **(B)** SHANK3 E71S mutant (chain A) with αCaMKII (chain B).

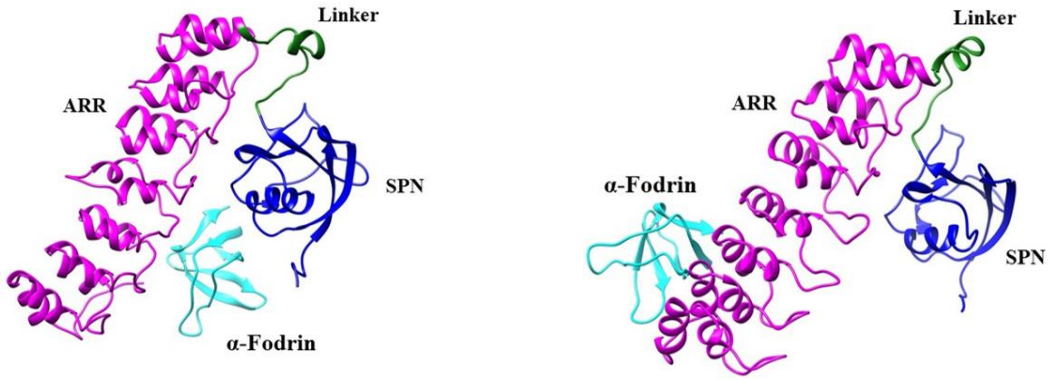

(A) **(B)**

Figure S3. The docking interaction between **(A)** SHANK3 WT protein and α-Fodrin; **(B)** SHANK3 E71S mutant and α-Fodrin.

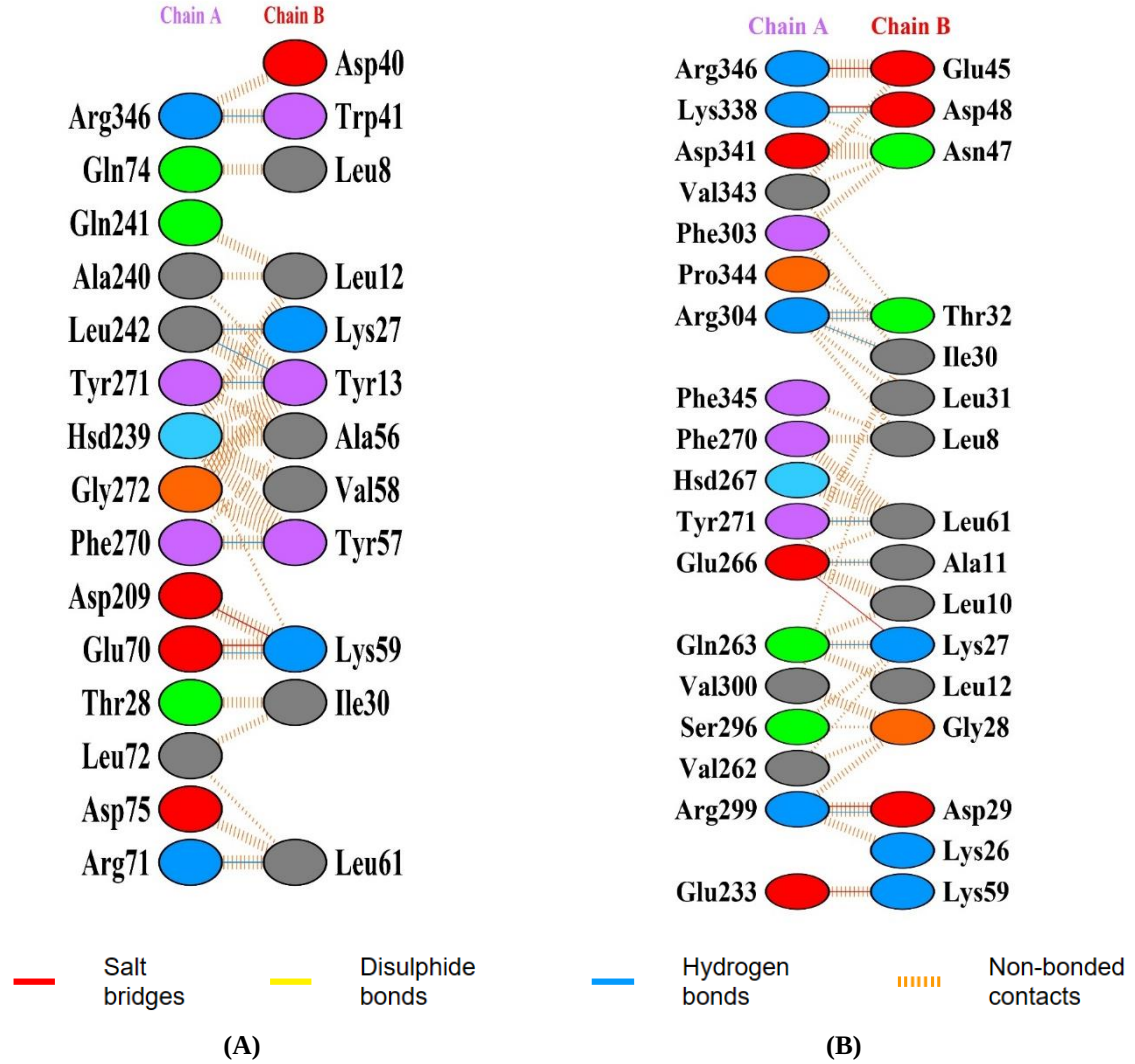

(A) **(B)**

Figure S4. The interactions between **(A)** SHANK3 WT protein (chain A) with α-Fodrin (chain B); **(B)** SHANK3 E71S mutant (chain A) with α-Fodrin (chain B).

Table S1. The interface statistics in SHANK3 WT protein with αCaMKII

Chain	No. of interface residues	Interface area (A^2)	No. of salt bridges	No. of disulfide bonds	No. of hydrogen bonds	No. of non-bonded contacts
A (SHANK3 WT)	27	1476	4	-	15	202
B (αCaMKII)	30	1448				

Table S2. The interface statistics in the SHANK3 E71S mutant αCaMKII

Chain	No. of interface residues	Interface area (A^2)	No. of salt bridges	No. ofdisulfide bonds	No. of hydrogen bonds	No. of non-bonded contacts
A (SHANK3 E71S)	17	824	3	-	7	96
B (αCaMKII)	15	862				

Table S3. The interface statistics in SHANK3 WT protein with α-Fodrin

Chain	No. of interface residues	Interface area (A^2)	No. of salt bridges	No. of disulfide bonds	No. of hydrogen bonds	No. of non-bonded contacts
A (SHANK3 WT)	15	661	2	-	7	99
B (α-Fodrin)	12	707				

Table S4. The interface statistics in the SHANK3 E71S mutant α-Fodrin

Chain	No. of interface residues	Interface area (A^2)	No. of salt bridges	No. of disulfide bonds	No. of hydrogen bonds	No. of non-bonded contacts
A (SHANK3 E71S)	18	800	5	-	8	125
B (α-Fodrin)	16	852				

Table S5. The different types of interactions between SPN and ARR domains in SHANK3 wild-type protein.

SPN	ARR	Distance	Possible interaction_forces
PRO:31	GLN:242	7.823	induction + dispersion
TRP:33	ASP:177	7.436	anion-π stacking,π-π stacking, hydrogen bond
TRP:33	ARG:179	6.52	cation-π stacking
TRP:33	LYS:212	5.986	cation-π stacking, hydrophobic
TRP:33	GLN:242	5.785	hydrogen bond,π-π stacking,dipole-π stacking
LYS:36	ASP:177	7.726	salt bridge, hydrogen bond
LYS:36	ARG:179	4.253	ionic repulsion CAUTION: possible repulsion
GLN:48	ARG:181	6.416	electrostatic: ion-dipole, hydrogen bond
ASP:49	HIS:144	5.277	salt bridge, hydrogen bond,anion-π stacking
ASP:49	PHE:178	7.279	anion-π stacking
ASP:49	ARG:179	7.432	salt bridge, hydrogen bond
ASP:49	THR:180	6.604	electrostatic: ion-dipole, hydrogen bond
ASP:49	ARG:181	2.981	salt bridge, hydrogen bond
ASP:49	ASP:182	7.432	ionic repulsion CAUTION: possible repulsion
ALA:50	ARG:179	5.551	induction + dispersion
LEU:51	HIS:144	7.718	induction + dispersion
LEU:51	ASP:177	4.818	induction + dispersion
LEU:51	PHE:178	5.858	hydrophobic
LEU:51	ARG:179	2.888	induction + dispersion
LEU:51	THR:180	5.977	induction + dispersion
LEU:51	ARG:181	6.286	induction + dispersion
LEU:51	ASP:182	5.979	induction + dispersion
LEU:51	GLY:183	4.377	hydrophobic
LEU:51	LEU:184	6.477	hydrophobic
LEU:51	THR:185	7.465	induction + dispersion
LEU:51	LYS:212	6.116	hydrophobic
LEU:51	ASP:213	5.007	induction + dispersion
LEU:51	SER:214	4.132	induction + dispersion
LEU:51	ARG:215	6.378	induction + dispersion
LEU:51	GLY:216	7.481	hydrophobic
ASN:52	ASN:142	6.821	electrostatic: dipole-dipole, hydrogen bond
ASN:52	PHE:143	7.818	π-π stacking
ASN:52	HIS:144	3.87	electrostatic: ion-dipole, hydrogen bond,π-π stacking, dipole-π stacking
ASN:52	GLY:149	7.909	induction + dispersion
ASN:52	CYS:151	7.349	electrostatic: dipole-dipole, hydrogen bond
ASN:52	HIS:175	7.036	electrostatic: ion-dipole, hydrogen bond,π-π stacking, dipole-π stacking
ASN:52	ASP:177	4.419	electrostatic: ion-dipole, hydrogen bond
ASN:52	PHE:178	3.7	π-π stacking
ASN:52	ARG:179	2.904	electrostatic: ion-dipole, hydrogen bond
ASN:52	THR:180	4.456	electrostatic: dipole-dipole, hydrogen bond
ASN:52	ARG:181	5.685	electrostatic: ion-dipole, hydrogen bond
ASN:52	ASP:182	7.298	electrostatic: ion-dipole, hydrogen bond
ASN:52	GLY:183	6.476	induction + dispersion
ASN:52	LEU:184	6.938	induction + dispersion

SPN	ARR	Distance	Possible interaction_forces
ASN:52	THR:185	7.484	electrostatic: dipole-dipole, hydrogen bond
TYR:53	HIS:175	7.215	cation-π stacking,π-π stacking ,hydrogen bond, dipole =-π stacking
TYR:53	ASP:177	6.704	anion-π stacking,π-π stacking, electrostatic: ion-dipole, hydrogen bond
TYR:53	PHE:178	7.044	π-π stacking,hydrophobic,dipole-π stacking
TYR:53	ARG:179	6.455	cation-π stacking,π-π stacking, hydrogen bond
GLY:54	HIS:175	7.333	induction + dispersion
LEU:55	HIS:175	7.975	induction + dispersion
PHE:56	HIS:175	7.64	cation-π stacking,π-π stacking
LYS:66	HIS:175	7.556	ionic repulsion CAUTION: possible repulsion hydrogen bond
PHE:67	ASP:140	7.975	anion-π stacking
PHE:67	ASN:142	7.496	π-π stacking
PHE:67	GLY:173	7.537	hydrophobic
PHE:67	HIS:175	3.514	cation-π stacking,π-π stacking
LEU:68	HIS:175	6.348	induction + dispersion
LEU:68	ASP:177	6.973	induction + dispersion
ASP:69	ARG:170	7.625	salt bridge, hydrogen bond
ASP:69	HIS:175	7.305	salt bridge, hydrogen bond,anion-π stacking
ASP:69	LEU:176	6.593	induction + dispersion
ASP:69	ASP:177	3.959	ionic repulsion CAUTION: possible repulsion
ASP:69	GLY:206	6.038	induction + dispersion
ASP:69	ALA:207	7.853	induction + dispersion
ASP:69	SER:208	6.331	electrostatic: ion-dipole, hydrogen bond,
ASP:69	TYR:211	5.102	anion-π stacking,π-π stacking, electrostatic: ion-dipole, hydrogen bond
GLU:70	HIS:175	7.948	salt bridge, hydrogen bond,anion-π stacking,
GLU:70	ASP:177	4.067	ionic repulsion CAUTION: possible repulsion
GLU:70	PHE:178	7.23	anion-π stacking
GLU:70	ARG:179	3.874	salt bridge, hydrogen bond
GLU:70	TYR:211	7.357	anion-π stacking,π-π stacking, electrostatic: ion-dipole, hydrogen bond
GLU:71	ASP:177	5.423	ionic repulsion CAUTION: possible repulsion
GLU:71	GLY:206	5.279	induction + dispersion
GLU:71	ALA:207	6.179	induction + dispersion
GLU:71	SER:208	2.702	electrostatic: ion-dipole, hydrogen bond
GLU:71	PRO:209	6.494	induction + dispersion
GLU:71	ASP:210	4.192	ionic repulsion CAUTION: possible repulsion
GLU:71	TYR:211	3.717	anion-π stacking,π-π stacking, electrostatic:ion-dipole, hydrogen bond
GLU:71	LYS:212	7.295	salt bridge, hydrogen bond
ARG:72	ASP:177	7.995	salt bridge, hydrogen bond
ARG:72	SER:208	7.667	electrostatic: ion-dipole, hydrogen bond,
ARG:91	HIS:175	7.742	ionic repulsion CAUTION: possible repulsion hydrogen bond,cation-π stacking,
TYR:92	ASP:140	5.225	anion-π stacking,π-π stacking, electrostatic, ion-dipole, hydrogen bond
TYR:92	PRO:141	7.208	hydrophobic
TYR:92	ASN:142	2.9	electrostatic: dipole-dipole, hydrogen bond,π=-π stacking,dipole-π stacking
TYR:92	PHE:143	4.197	π-π stacking,hydrophobic,dipole-π stacking
TYR:92	HIS:144	3.716	cation-π stacking,π-π stacking,hydrogen bond,dipole=-πstacking
TYR:92	CYS:151	7.633	electrostatic: dipole-dipole, hydrogen bond
TYR:92	HIS:175	6.019	cation-π stacking,π-π stacking,hydrogen bond,dipole=-πstacking
TYR:92	PHE:178	3.555	π-π stacking,hydrophobic,dipole-π stacking
TYR:92	ARG:179	6.479	cation-π stacking,π-π stacking, hydrogen bond
TYR:92	ARG:181	5.998	cation-π stacking,π-π stacking, hydrogen bond